

The Dependence of the Plasmon Field Induced Nonradiative Electronic Relaxation Mechanisms on the Gold Shell Thickness in Vertically Aligned CdTe–Au Core–Shell Nanorods

Svetlana Neretina,^{†,II} Erik C. Dreaden,[†] Wei Qian,[†] and Mostafa A. El-Sayed^{*†}

Laser Dynamics Laboratory, School of Chemistry and Biochemistry, Georgia Institute of Technology, Atlanta, Georgia 30332-0400; and Department of Mechanical Engineering, Temple University, 1947 N. 12th St., Philadelphia, PA 19122

Robert A. Hughes,[‡] John S. Preston,^{‡,§} and Peter Mascher[§]

Brockhouse Institute for Materials Research, McMaster University, Hamilton, Ontario, L8S 4M1, Canada; and Department of Engineering Physics, McMaster University, Hamilton, Ontario, L8S 4L7, Canada

Received June 18, 2009; Revised Manuscript Received August 15, 2009

ABSTRACT

The dependence of the plasmon field enhancement of the nonradiative relaxation rate of the band gap electrons in vertically aligned CdTe–Au core–shell nanorods on the plasmonic gold nanoshell thickness is examined. Increasing the thickness of the gold nanoshell from 15 to 26 nm is found to change the decay curve from being nonexponential and anisotropic to one that is fully exponential and isotropic (i.e., independent of the nanorod orientation with respect to the exciting light polarization direction). Analysis of the kinetics of the possible electronic relaxation enhancement mechanisms is carried out, and DDA simulated properties of the induced plasmonic field of the thin and thick gold nanoshells are determined. On the basis of the conclusions of these treatments and the experimental results, it is concluded that by increasing the nanoshell thickness the relaxation processes evolve from multiple enhancement mechanisms, dominated by highly anisotropic Auger processes, to mechanism(s) involving first-order excited electron ejection process(es). The former is shown to give rise to nonexponential anisotropic decays in the dipolar plasmon field of the thin nanoshell, while the latter exhibits an exponential isotropic decay in the unpolarized plasmonic field of the thick nanoshell.

Thin-film-based devices, such as transistors, solar cells, light-emitting diodes and solid-state lasers, are now a ubiquitous part of modern societies. Essential to all of these devices is the formation of interfaces between dissimilar materials. Such interfaces give rise to properties which are different from those of the individual bulk materials. Thus, it stands to reason that nanostructures having interfaces between dissimilar materials should prove equally rewarding in terms of device architectures. In this case, the large surface to volume ratios of the nanoparticles have the potential to give

rise to interfacial phenomenon which overwhelm the properties of the entire nanostructure. So, even though the nanostructure contains chemically distinct regions, its properties may be more aptly described in terms of a hybrid response.

The localized surface plasmon resonances, accessible through the optical excitation of noble metal nanoparticles (Au, Ag), offer intriguing possibilities in terms of forming such hybrid nanostructures. Not only do these plasmonic nanomaterials strongly interact with light, but the excitation gives rise to near-fields which extend well beyond their physical dimensions. Thus, there exists the strong possibility that these plasmon oscillations will fundamentally alter the properties of nearby nanomaterials. Already there exist numerous examples where the plasmonic fields of noble metal nanoparticles, placed in close proximity to semiconductors, have fundamentally altered both the radiative and

* Corresponding author: e-mail, melsayed@gatech.edu; telephone, 404-894-0292.

[†] Laser Dynamics Laboratory, School of Chemistry and Biochemistry, Georgia Institute of Technology.

[‡] Department of Mechanical Engineering, Temple University.

[§] Brockhouse Institute for Materials Research, McMaster University.

^{II} Department of Engineering Physics, McMaster University.

nonradiative properties of the semiconductor. Important examples include the observed enhancements of (i) solar cell efficiencies,^{1–3} (ii) the photoluminescence in semiconducting nanoparticles,^{4,5} (iii) the nonradiative relaxation rate in semiconductor nanorods,^{6,7} (iv) the emission from light-emitting diodes,^{8,9} and (v) the rates of the primary step (retinal isomerization and the proton pump)^{10,11} in the other photosynthetic system in nature, bacteriorhodopsin.

The versatility and tunability of standalone plasmonic nanoparticles have now been decisively demonstrated.¹² This is, in large part, due to the extraordinary advancements in the fabrication of plasmonic nanoparticles, where there now exists considerable control over shape and size. Nanospheres,¹³ rods,¹⁴ shells,¹⁵ disks,¹⁶ rings,¹⁷ stars,¹⁸ and cubes¹⁹ are now routinely fabricated. Of particular importance to this work are the plasmonic properties of nanoshells since core–shell nanorods, formed through the encapsulation of a semiconductor with a noble metal nanoshell, provide the most straightforward geometry for studying the hybrid response. Plasmonic spherical nanoshells have been extensively studied,^{20–22} exhibiting a large degree of tunability that greatly exceeds that of solid metallic nanospheres. With the capability to tune the resonant plasmon frequency through alterations to nanoshell shape, thickness, overall radius, and dielectric environment firmly established, it follows that the degree of coupling in a core–shell nanorod should also become highly tunable.

In a recent study,⁶ we reported on the decay of CdTe excitons in CdTe–Au core–shell nanorods (height = 200 nm, width = 100 nm) with a 15 nm gold shell thickness. It was determined that the exciton decay rate is sensitive to the surface plasmon field of the gold nanoshell. In a subsequent study⁷ we varied the strength of the surface plasmon field by varying the tilt angle of the core–shell nanorods with respect to the polarization direction of the exciting light. For the gold nanoshell thickness used, the plasmon polarization at the band gap absorption edge was shown, through discrete dipole approximation (DDA) simulations, to be dipolar in nature and mostly polarized along the long axis of the nanorod. The core–shell structures showed a highly anisotropic response characterized by an enhanced exciton decay rate for low tilt angles which grew progressively stronger as the tilt angle was increased. The decay curves exhibit nonexponential behavior with a shape that is quite sensitive to the tilt angle. Such a response indicates the presence of more than one relaxation mechanism, but one will be dominated when there exists a high degree of alignment between the plasmon field direction and the moment of the band gap exciton electronic transition. For this dominant mechanism, occurring at high tilt angle, the relaxation mechanism is described in terms of an enhanced radiative bandgap absorption followed by Auger type (i.e., an exciton–exciton annihilation) relaxation processes.

In the present report, we describe our attempt to increase the plasmon field effects in the vertically aligned CdTe–Au core–shell nanorods by tuning the extinction maximum of the plasmon nanoshell to the band gap transition of CdTe

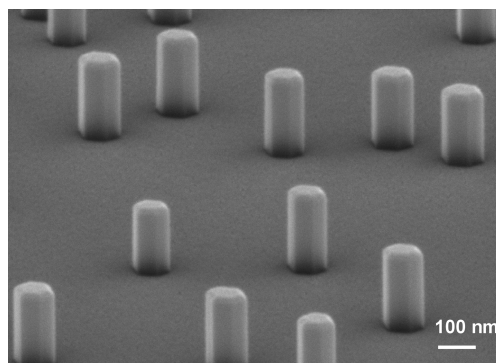


Figure 1. SEM image of the vertically aligned CdTe–Au core–shell nanorods. The nanorods shown have an aspect ratio near 2 (height = 200 nm, width = 100 nm) and a gold shell thickness of 15 nm.

by increasing the shell thickness. Such structures did not behave as anticipated but instead showed a band gap electronic excitation that decays in a purely exponential manner with a decay constant that is not much larger than that found for the thin nanoshell rod. The decay is also found to be isotropic and does not depend on the relative orientation of the polarization direction of the exciting laser light and the long axis of the core–shell nanorod.

The kinetics of the possible decay mechanisms as well as the plasmon field properties (i.e., polarization and relative absorption vs scattering cross section) determine the shape of the decay and its anisotropic behavior. From the results of the kinetic analysis, as well as the DDA simulations of the plasmon field properties, it is concluded that the mechanisms and the plasmon field properties vary greatly with an increasing nanoshell thickness. This leads to a change in the mechanisms from being combined Auger-type and electron ejection mechanisms in thin nanoshell rods to just an electron ejection mechanism in the thick nanoshell.

Sample Preparation. The fabrication of the vertically aligned core–shell nanostructures used in these studies is described elsewhere.^{23,24} Briefly, the CdTe nanorod cores were deposited using a vapor–liquid–solid (VLS) growth mode. The single crystal CdTe nanorods produced exhibit a wurtzite crystal structure with its *c*-axis normal to and sharing an epitaxial relationship with the [0001] sapphire substrate. Subsequent to nanowire growth a gold shell is sputtered onto the nanorods to the desired thickness using a sputter coater operating at room temperature. For the measurements presented here the thickness of the gold shell was varied by adding gold to a preexisting shell with spectroscopic characterization performed for each thickness. Figure 1 shows a scanning electron microscopy (SEM) image of the core–shell nanostructures used.

Optimization of the Gold Nanoshell Plasmon Field Strength at the CdTe Band Gap Energy through the DDA Simulations. In order to increase the plasmon field strength at the band gap energy, we used DDA simulations to determine the thickness for which there exists an extinction maximum at this energy, an energy which also corresponds to the laser wavelength used (770 nm). The discrete dipole approximation^{25–29} has been used for theoretically predicting

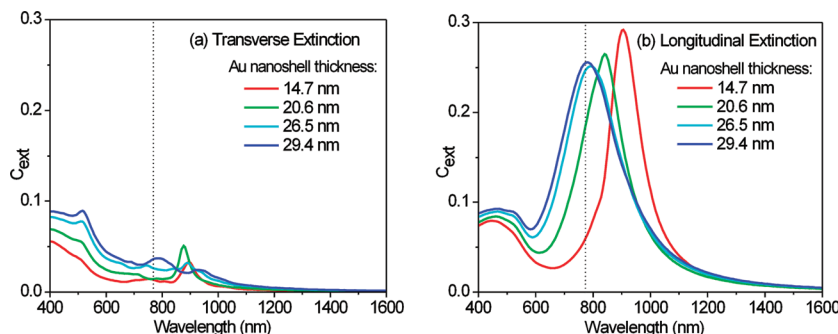


Figure 2. DDA simulations showing the wavelength dependence of the (a) transverse and (b) longitudinal extinction cross sections for gold nanoshells of various thicknesses which encapsulate a CdTe core (diameter = 74 nm, height = 184 nm). The dashed line denotes the CdTe band gap edge at 770 nm. Note that the intense longitudinal extinction peak blue-shifts toward 770 nm as the shell thickness is increased. The vertical axes of both plots are identical in order to facilitate comparisons.

the response of plasmonic nanostructures to the incident electromagnetic radiation. The technique, which is described in detail elsewhere,^{30,31} is a method based on computational electrodynamics where the target particle and its surroundings are described in terms of a cubic array of point dipoles and has proven widely applicable in predicting the optical response of plasmonic nanostructures of varying size, shape, and dielectric environment.^{6,7,32–36} It was used to calculate the angular- and thickness-dependent optical properties of the CdTe–Au core–shell nanostructures where the core and shell dimensions were experimentally determined by SEM and tapping-mode atomic force microscopy (AFM), respectively. Calculations were performed for 184×74 nm hemispherically capped, cylindrical CdTe cores with Au shells of varying thicknesses covering all sides but the flat base ($\sim 10^5$ total dipoles). Experimentally determined complex refractive indices for Au³⁷ and CdTe³⁸ were applied in an in vacuo environment with the degree of tilt defined as the angle between the incident propagation vector \vec{k} and the nanorod longitudinal axis.

Figure 2 shows the DDA simulation results of the gold nanoshell extinction cross section as a function of wavelength for a semiconductor core encapsulated with gold shells of various thicknesses for the exciting light polarized in the transverse (Figure 2a) and longitudinal (Figure 2b) directions. The figures clearly show the presence of an intense longitudinal extinction in 700–1000 nm wavelength range. The transverse extinction is considerably weaker and exhibits no prominent peaks. Of particular importance is the fact that the intense longitudinal extinction peak shows a substantial blue shift as the shell thickness around the CdTe core is increased. Of note, is that the extinction peak exhibits a resonance near the desired 770 nm CdTe band gap energy for a shell thickness in the 26–29 nm range. This is made more evident in Figure 3 which shows the extinction cross sections calculated at 770 nm for the transverse and longitudinal plasmon modes as a function of the gold nanoshell thickness. On the basis of these simulations, core–shell nanorods were fabricated with a shell thickness of 26 nm and spectroscopically characterized. The chosen thickness provides a high level of overlap between the extinction maximum and the CdTe band gap, while at the same time minimizing the attenuation of light by the gold

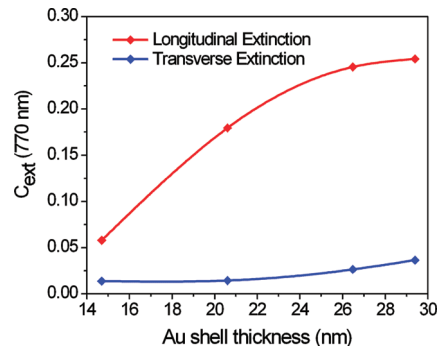


Figure 3. Calculated longitudinal (red) and transverse (blue) extinction cross sections at the 770 nm band gap edge of CdTe as a function of the gold nanoshell thickness. Note that the extinction of the longitudinal mode is near maximal for gold shell thicknesses greater than 26 nm.

shell and, thus, allowing for a higher level of interaction with the semiconductor core.

Pump–Probe Experimental Setup. The experimental configuration, as well as the femtosecond pump–probe apparatus, has been described in detail elsewhere.⁶ Briefly stated, the core–shell nanorods are optically pumped with 400 nm pulses while temporally monitoring the relaxation of the excited carriers with a 770 nm probe beam. The wavelength of the probe beam was chosen to coincide with the band gap edge of CdTe. The transient bleach intensities of the core in the core–shell nanorod were measured from the changes in the intensity of the probe beam at different times after the pump pulse excitation and at a variety of tilt angles such that the 0° tilt illuminates only the tops of the core–shell structures while higher tilt angles increasingly illuminate the sidewalls as is shown schematically in Figure 4. Thus, sample tilting allows one to monitor the electronic relaxation within the CdTe core as the plasmon excitation associated with the core–shell nanorod varies from transverse (i.e., 0° tilt) to longitudinal (i.e., 90° tilt). It should be noted that both the pump and probe beams are linearly polarized such that the polarization direction lies along the length of the tilted core–shell nanorod.

Experimental Results. Figure 5 shows the room temperature transient bleach intensities obtained for core–shell nanorods with shell thicknesses of 15 nm (Figure 5a) and 26 nm (Figure 5b). For the thinner shells the decay curves

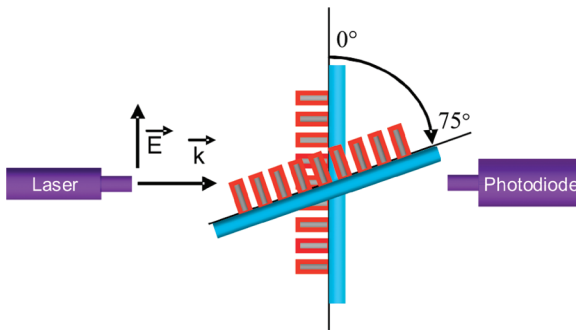


Figure 4. Schematic showing the experimental configuration used to examine the anisotropy of the plasmon field effects on the nonradiative relaxation of the CdTe band gap electrons. Anisotropy can be probed by changing the relative orientation of the nanorods with respect to the exciting laser light polarization. The linearly polarized light for both the pump and probe pulses have a parallel propagation vector k and an electric field E_{light} . The light is directed at a sample which can be tilted from 0 to 75° away from the polarization direction of the exciting light electric field. CdTe, gold, and the sapphire substrate are shown in gray, red, and blue, respectively.

are very nonexponential and highly anisotropic, exhibiting an exciton nonradiative average electronic relaxation time which decreases from 3 to 0.9 ps as the core–shell nanorods are tilted from 0° to 75°. The shape of the nonexponential decay curve is almost linear for a 0° tilt angle but becomes more exponential-like as the tilt angle is increased to 75°. Surprisingly, for the thicker shell, where there exists a maximum overlap between the longitudinal plasmon mode and the band gap edge of CdTe, there exists an isotropic response characterized by tilt-independent relaxation times of approximately 1.3 ps. Also, in contrast to the results for the thin shell, the thick shell nanorods show an exciton decay mode which is purely exponential in nature. The lack of the angle dependence of the kinetics in the thick shell nanorods may be explained by assuming that the observed transient bleach decay signal is from hot electron relaxation in the metallic gold nanoshell. However, it is well-known that the recovery of transient bleach signal from metallic nanopar-

ticles is characterized by two processes, electron–phonon and phonon–phonon relaxation processes with decay times being a few picoseconds and several hundred picoseconds, respectively. Therefore, if there is contribution from the gold nanoshell to the overall signal, we should have seen the signal decay to a level above zero when the observation window was limited to less than 10 ps as in our case. However, as is shown in Figure 5b, all the signals decay very rapidly to zero. This indicates that we do not observe dynamics associated with the gold nanoshell in our experiments. The remainder of our report details how these dramatic changes in the nature of the decay (and thus the mechanisms involved) can be explained in terms of the different plasmon field properties associated with gold nanoshells of various thicknesses and the different decay kinetics of the various mechanisms involved.

Two Types of Possible Mechanisms Leading to Enhanced Decay. The two proposed mechanisms⁶ responsible for the plasmon field enhancement of the nonradiative relaxation of the semiconductor excitons in CdTe–Au core–shell nanorods are shown schematically in Figure 6. The excited electron ejection (EEE) mechanism (Figure 6a) describes a process where the ejection (i.e., the removal) of the excited electron occurs through its ionization via the absorption of one or two photons from the plasmon field or the laser monitoring light (as the plasmon field greatly enhances the absorption properties of the semiconductor) or through its stimulated emission. For the Auger mechanism (Figure 6b) a ground state electron absorbs a photon from the plasmon field or the laser monitoring light, promoting it to an excited state and, thus, increasing the exciton density. One of the excitons (an electron–hole pair) then recombines giving up its binding energy to the other exciton leading to its dissociation. While the two mechanisms share many similarities, it is important to note that the Auger process relies on a ground state electronic transition, whose moment is along the nanorod long axis, while the excited electron ejection mechanism relies solely on a transition of the excited state electron to either the continuum or the gold shell. A further examination of these

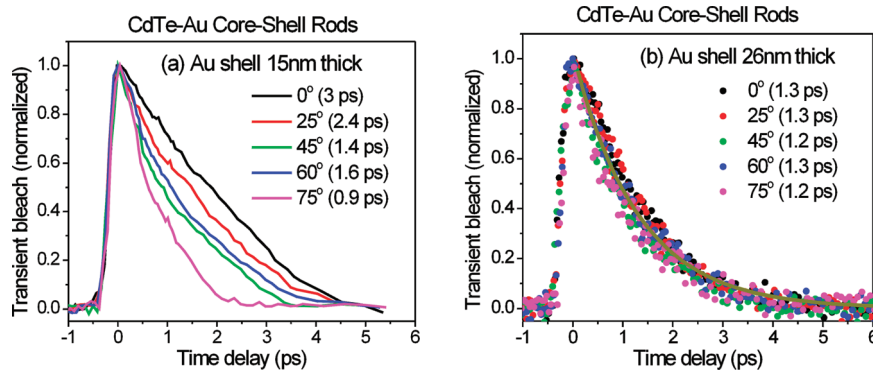


Figure 5. The temporal dependence of the transient bleach intensity at the semiconductor band gap energy as a function of tilt angle for CdTe–Au core–shell nanorods with shell thicknesses of (a) 15 nm and (b) 26 nm. A comparison of the data for the two gold nanoshell thicknesses shows obvious differences in the angular dependence of the semiconductor nanorod exciton decay. The thin gold shell gives enhanced exciton decay that is very nonexponential where the shape changes with the tilt angle. Such a response suggests the involvement of multiple decay mechanisms where one or more of these mechanisms are anisotropic (i.e., enhancing the exciton absorption along the long axis followed by rapid Auger processes⁷). The thick shell, on the other hand, exhibits an isotropic exponential behavior indicative of single or multiple mechanisms where the kinetics is first order in nature.

processes and their associated rate equations proves this difference to be crucial in determining not only the shape but also the anisotropy of the observed decay curves.

Decay Kinetics of the Different Mechanisms. The EEE mechanism involves the ejection (i.e., the removal) of the excited electron in the band gap excitation process. This can involve its ionization to the continuum state or to the gold conduction band, or alternatively, it can simply occur by stimulating it in a manner which causes it to emit and then return to the ground state. For the EEE mechanism the rate of the decay of the excited electron in the band gap state is given by

$$-\frac{d[E_1]}{dt} = k_{\text{EEE}}[E_1] \quad (1)$$

where $[E_1]$ is the concentration of the excited electrons in the band gap state and k_{EEE} is the rate constant of the EEE process. Rearranging and integrating the rate expression (1) gives the first-order decay of $[E_1]$

$$[E_1]_t = [E_1]_0 e^{-k_{\text{EEE}}t} \quad (2)$$

where $k_{\text{EEE}} = 1/\tau_{\text{EEE}}$ and τ_{EEE} is the observed lifetime of the state if it is completely determined by the enhanced rate mechanism. It is clear from eq 2 that the EEE mechanism gives rise to an exponential decay of the band gap excited state (i.e., excitons).

For the Auger mechanism at an excitation level for which only one electron–hole pair dominates the observed annihilation process, the rate of the decay is given by

$$-\frac{d[E_1]}{dt} = k_{\text{annh}}[E_1][E_1] \quad (3)$$

where k_{annh} is the rate constant of the exciton annihilation process. Rearranging and integrating eq 3 gives the decay of $[E_1]$ which has the form

$$\frac{1}{[E_1]_t} = \frac{1}{[E_1]_0} + k_{\text{annh}}t \quad (4)$$

If the rate of the excitation of the CdTe band gap electron (this could be high due to the plasmon enhancement) equals the rate of its annihilation (i.e., assuming that the steady state approximation holds), then eq 3 becomes

$$-\frac{d[E_1]}{dt} = k_{\text{abs}}[\text{CdTe}] = k'_{\text{abs}} \quad (5)$$

where k_{abs} is the rate constant of the absorption of light by CdTe solid, $[\text{CdTe}]$ is the density of CdTe solid, and k'_{abs} is, thus, the effective absorption rate of the CdTe semiconductor. Rearranging and integrating eq 5 gives the decay of the excited electron in the $[E_1]$ state

$$[E_1]_t = [E_1]_0 - k'_{\text{abs}}t \quad (6)$$

which is a linear-type decay in which the excited state concentration decreases linearly with time. At very high levels of femtosecond laser excitation, for which more than two electron–hole pairs are formed, it has been shown that the decay could become exponential.³⁹ The

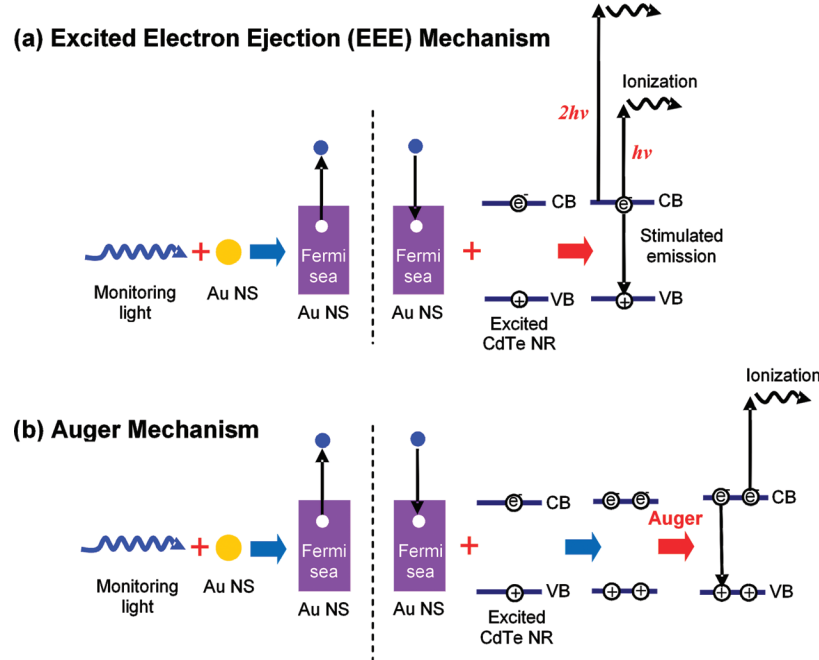


Figure 6. Schematic diagram showing both the (a) excited electron ejection (EEE) and (b) the Auger mechanisms. For both mechanisms the incident laser light excites the surface plasmon resonance oscillations in the gold nanoparticle (NS) producing strong fields which can facilitate or enhance the absorption or stimulated emission within the semiconductor nanorod (NR). Note that the excited electron ejection mechanism (EEE) involves an excited state absorption or stimulated emission while the Auger process involves ground state absorption.

laser power used in the present work is not in this limit. From eqs 4 and 6 and at the pump laser power used in our work, the Auger mechanism yields a nonexponential decay.

The above kinetically based conclusions can, therefore, assist in determining the type of mechanism involved in the plasmon enhancement processes since each mechanism gives rise to a decay curve of different shape. Thus, if the decay is exponential, then electron ejection mechanism(s) are involved, while if it is nonexponential then the Auger mechanism is dominant (provided that the laser excitation levels are reasonable). If the decay is nonexponential and its shape is sensitive to the tilt angle, then a mixture of mechanisms is involved where one mechanism is sensitive to the polarization of the plasmon field (see next section).

The Polarization Dependence of the Decay Curves. The shape of the observed decay gives the dependence of $[E_1]$ on time. If the mechanism involved also has a dependence on the tilt angle, then the observed decay constant (k) also has such a dependence. In order to examine the dependence of the value of k on the tilt angle, we have to examine its expression in terms of quantum mechanical integrals. Below we examine the prediction of the different mechanisms with regard to the angular dependence of the excitation process. For the EEE mechanism k_{EEE} is given by

$$k_{\text{EEE}} = C' \left| \vec{E}_{\text{plasm}} \cdot \vec{\mu}_{1-f} \right|^2 \quad (7)$$

where \vec{E}_{plasm} is the plasmon enhanced electromagnetic field which ejects the electron, $\vec{\mu}_{1-f}$ is the moment of the transition from the band gap excited state to the final state, where the ejected electron is ejected, and C' is a constant. The integral of eq 7 predicts that the decay will depend on the tilt angle between the exciting light polarization direction and the long axis of the nanorod only if the plasmon is polarized and the transition moment is along a fixed direction in the nanorod. However, if either \vec{E}_{plasm} or $\vec{\mu}_{1-f}$ is nondirectional (i.e., not a vector), the decay will not depend on the tilt angle. The EEE mechanism is expected to be isotropic if the ejection of the electron is to a continuum state even if the plasmon field is polarized. The moments of the allowed electronic transitions between the planes containing Te^{2-} and those containing the Cd^{2+} are along the long axis of the CdTe nanorod which corresponds to the c -axis of wurtzite crystal structure. Thus, the radiation coupling between the plasmon field of the gold shell and the CdTe core of the semiconductor is strongest when these two are parallel. This coupling is maximum if \vec{E}_{plasm} is dipolar and polarized along the long axis. Since \vec{E}_{plasm} is excited by the exciting light, its value is expected to depend on the square of the dot product of the two fields (i.e., on $|\vec{E}_{\text{plasm}} \cdot \vec{E}_{\text{light}}|^2$). This could give rise to a decay curve which is sensitive to the relative orientation of the nanorod (if it has a nanoshell with a dipolar plasmon field) and the polarization direction of the monitoring light (in the lab coordinates). If the plasmon field is unpolarized, its strength will, of course, be independent of the exciting light direction giving rise to isotropic decay.

For the Auger mechanism, the rate of exciton annihilation depends on the square of the exciton concentration which

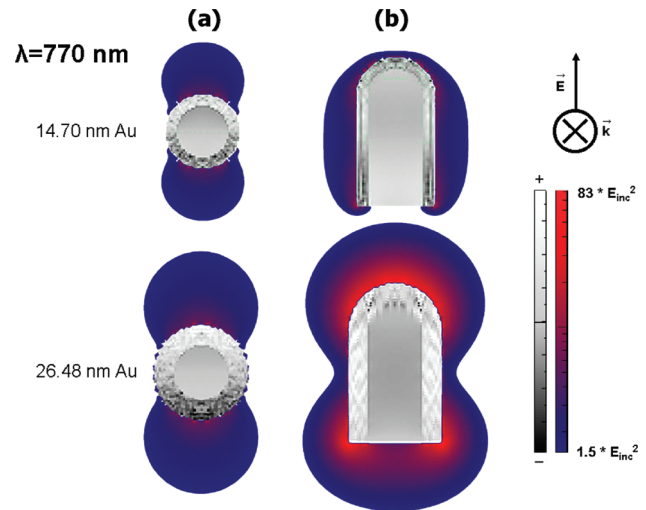


Figure 7. Calculated plasmonic field enhancement (color contours) and normalized induced polarization parallel to the exciton transition moment (grayscale) for CdTe–Au core–shell nanorods with identically shaped cores and varying shell thickness. The plasmon field distributions shown are those produced in the (a) transverse and (b) longitudinal configuration under 770 nm excitation. Note that for the longitudinal configuration the plasmon field is dipolar in character for the thin gold nanoshell and unpolarized for the thick gold nanoshell. In the thin gold nanoshell the upper and bottom halves are oppositely charged as a result of the surface plasmon oscillations. This, however, is not the case for the thick gold nanoshell where the charge distribution is homogeneous.

depends on the rate of absorption of the ground state semiconductor at the band gap wavelength. The rate of absorption is given by

$$k_{\text{abs}}[\text{CdTe}] = C'' \left| \vec{E}_{\text{plasm}} \cdot \vec{\mu}_{01} \right|^2 [\text{CdTe}] \quad (8)$$

where $\vec{\mu}_{01}$ is the moment of the transition from the ground state to the excited state and C'' is a constant. Since $\vec{\mu}_{01}$ (the band gap transition moment) is along the long axis of the CdTe nanorod, then k_{annh} will be maximum when the plasmon field polarization direction is also along the long axis of the nanorod. However, if the plasmon field is unpolarized, then k_{annh} and, thus, the decay of the Auger mechanism will be isotropic and insensitive to the tilt angle.

Dependence of the Plasmonic Field Polarization on the Gold Nanoshell Thickness As Determined by DDA Simulations. Electric field enhancement and induced polarization parallel to the CdTe transition moment were calculated using codes provided by S. Li and G. C. Schatz (Northwestern University). Figure 7 compares the DDA simulated polarization (white and black) within the gold shell and the semiconductor core as well as the gold surface plasmon field enhancement (in blue and red colors) of the thin (15 nm) and thick (26 nm) gold shells. From the Figure 7 it is clear that, while the plasmon field is dipolar in the thin shell nanorod, it is almost unpolarized in the thick shell nanorod.

These simulation results could explain the lack of anisotropy observed in the decay curves of the thick shell nanorod due to the unpolarized nature of the plasmon field. It does

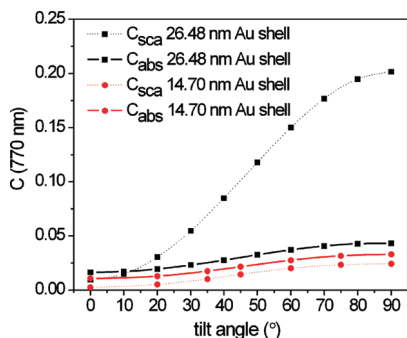


Figure 8. The DDA calculated angular-dependent absorption (solid) and scattering (dotted) cross sections for CdTe–Au core–shell structures excited at 770 nm for thin (red diamonds) and thick (black squares) gold nanoshells. Note that the scattering dramatically increases with shell thickness, while absorption remains relatively unchanged. Noteworthy, is the fact that as the nanoshell thickness is increased, the scattering at 770 nm increases dramatically as the tilt angle increases, thus eliminating the anisotropic Auger mechanism.

not, however, explain how the decay, which is nonexponential in the thin shell nanorods, becomes purely exponential for the thick shell rods. The nonexponential anisotropic decay in the thin nanoshell sample is likely due to the Auger mechanism which is expected to be nonexponential due to the dependence of its decay rate on the square of the concentration of excited states and the different time dependences of its decay shape under different levels of excitation. The fact that the shape of the nonexponential decay changes with tilt angle suggests the presence of another mechanism whose rate depends on the concentration of excited states raised to a power other than two. If it is a power of one it would suggest the EEE mechanism. If both mechanisms persist in the thick shell nanorods, the decay should have been nonexponential. The fact that it is exponential suggests that the Auger mechanism is either not important or that multiple excitation electron–hole pairs are formed in the thick nanoshell sample. The latter, however, is considered unlikely at the laser pump power levels used in experiments described here.

Relative Yield Dependence of Enhanced Absorption vs Enhanced Scattering of the Exciting Light by the Plasmon Field on the Gold Nanoshell Thickness. As shown in Figure 8, the scattering cross section of the CdTe nanorods with the thick gold nanoshell is extremely large. At first, we thought that the disappearance of the angle dependence of the transient bleach signal from the thick shell nanorods is due to the depolarization of the incident excitation light by frequent scattering within the arrays of the nanorods. However, the theoretical calculation displayed in the Figure 7 shows that the longitudinal plasmon field for the thick gold nanoshell is unpolarized in character. Thus, actually, we do not need to propose mechanism involving the scattering of the incident light to depolarize the light, as this would require a special cavity to confine the scattered light in the space occupied by the nanorods. Insight into why the Auger mechanism might become unimportant for the thick gold nanoshell is gained from the result shown in Figures 8. The DDA derived extinction curves for the 90° tilt angle are

decomposed into their absorption and scattering yields for nanoshells of varying thicknesses. The figure shows that the scattering yield increases rapidly with tilt angle for the thick nanoshell, suggesting that the concentration of excitons also decreases rapidly with tilt. Since the rate of the Auger process depends on the square of the exciton concentration, the contribution of this mechanism must fall rapidly with tilt. Furthermore, since the scattering is much greater in the thick nanoshell sample, the multiple excitation of electron–hole pairs (in which the decay can be exponential³⁹) becomes less likely than that for the thin shell. Thus, it seems that for the thick shell nanorods the Auger process is unimportant and the EEE mechanism dominates. The lack of anisotropy of this mechanism in the thick shell nanorod can, thus, be attributed to the unpolarized nature of the plasmon field.

Summary of the Results and Conclusions. Hybrid nanoparticles, comprised of two dissimilar materials, are expected to exhibit new properties due to their relatively large interface area to volume ratios. This is especially true if one of the nanomaterials is a noble metal capable of surface plasmon electronic oscillation which induce near-fields that extend well beyond its physical dimensions. Our recent studies examined the enhancement of the electronic relaxation processes for a semiconductor core exposed to the plasmonic fields associated with a gold shell. In the present work the effect of the thickness of the gold shell on the enhanced relaxation of the band gap excitation is examined. It is observed that the shape and anisotropy of the decay curves are sensitive to the gold nanoshell thickness. For the thin nanoshell (15 nm) the decay shapes were very nonexponential and changed significantly as the tilt angle between the nanorod long axis and the polarization of the exciting light was varied. The thick nanoshell (26 nm), on the other hand, gave rise to exponential decays with no tilt dependence.

It is concluded that the shape of the decay curves reflects the kinetics of the decay of the excited electron in the band gap excited state, where the exact nature of the kinetics depends on the process(es) involved. These new processes, which have been previously discussed, describe the enhanced ejection of the excited electron (either to the continuum, to the gold core, or to the ground state) or the enhanced ground state absorption followed by exciton–exciton annihilation (i.e., Auger processes). The electron ejection mechanism is shown here to give rise to exponential decay, while the Auger mechanism results in a nonexponential decay under our laser excitation conditions. It is, thus, concluded that the plasmon enhanced relaxation for the hybrid system with the thin nanoshell is due to the Auger mechanism, with additional contributions from the first-order ejection of the electrons. For the hybrid system with the thick nanoshell the Auger processes become unimportant. These conclusions are found to be in agreement with the predicted properties of the plasmonic field obtained from DDA simulations. It is also found that, while the plasmonic enhanced absorption and scattering processes are comparable and independent of tilt angle for the thin shell nanorods, the field enhancement for the thick shell nanorods is dominated by the scattering processes. This dominance is especially true at high tilt angles where one would expect the ground state absorption

needed for Auger processes to be maximized. Furthermore, the induced plasmonic field is found to be dipole polarized in the thin nanoshell but is unpolarized in the thick nanoshell. It is this difference which accounts for the observation that the decays are sensitive to the tilt angle in the thin shell nanorods (where there exists a highly polarized ground state absorption that is involved in the enhanced Auger relaxation process) but are insensitive to the tilt for the thick shell nanorods.

Acknowledgment. S.N. would like to acknowledge the financial support provided by the NSERC postdoctoral fellowship program. M.A.E. would like to thank the NSF-DMR (0906822). The McMaster University group would like to acknowledge the Canadian Institute for Advanced Research (CIFAR), the Natural Sciences and Engineering Research Council (NSERC), and the Ontario Research and Development Challenge Fund (ORDCF) under the auspices of the Ontario Photonics Consortium (OPC) for the funding provided and the Canadian Centre for Electron Microscopy (CCEM) for access to their facilities. We also acknowledge the assistance of Gabriel Devenyi with the gold depositions.

References

- (1) Schaadt, D. M.; Feng, B.; Yu, E. T. *Appl. Phys. Lett.* **2005**, *86*, 063106.
- (2) Pillai, S.; Catchpole, K. R.; Trupke, T.; Green, M. A. *J. Appl. Phys.* **2007**, *101*, 093105.
- (3) Sundararajan, S. P.; Grady, N. K.; Mirin, N.; Halas, N. J. *Nano Lett.* **2008**, *8*, 624–630.
- (4) Lee, J.; Govorov, A. O.; Dulka, J.; Kotov, N. A. *Nano Lett.* **2004**, *4*, 2323–2330.
- (5) Lee, J.; Hernandez, P.; Lee, J.; Govorov, A. O.; Kotov, N. A. *Nat. Mater.* **2007**, *6*, 291–295.
- (6) Neretina, S.; Qian, W.; Dreaden, E.; El-Sayed, M. A.; Hughes, R. A.; Preston, J. S.; Mascher, P. *Nano Lett.* **2008**, *8*, 2410–2418.
- (7) Neretina, S.; Qian, W.; Dreaden, E. C.; El-Sayed, M. A.; Hughes, R. A.; Preston, J. S.; Mascher, P. *Nano Lett.* **2009**, *9*, 1242–1248.
- (8) Vuckovic, J.; Loncar, M.; Scherer, A. *IEEE J. Quantum Electron.* **2000**, *36*, 1131–1144.
- (9) Catchpole, K. R.; Pillai, S. *J. Lumin.* **2006**, *121*, 315–318.
- (10) Biesso, A.; Qian, W.; El-Sayed, M. A. *J. Am. Chem. Soc.* **2008**, *130*, 3258–3259.
- (11) Biesso, A.; Qian, W.; El-Sayed, M. A. *J. Am. Chem. Soc.* **2009**, *131*, 2442.
- (12) Wang, H.; Brandl, D. W.; Nordlander, P.; Halas, N. J. *Acc. Chem. Res.* **2007**, *40*, 53–62.
- (13) Jana, N. R.; Gearheart, L.; Murphy, C. J. *Chem. Mater.* **2001**, *13*, 2313–2322.
- (14) Jana, N. R.; Gearheart, L.; Murphy, C. J. *J. Phys. Chem. B* **2001**, *105*, 4065–4067.
- (15) Oldenburg, S. J.; Averitt, R. D.; Westcott, S. L.; Halas, N. J. *Chem. Phys. Lett.* **1998**, *288*, 243–247.
- (16) Maillard, M.; Giorgio, S.; Pilani, M. P. *Adv. Mater.* **2002**, *14*, 1084–1086.
- (17) Aizpurua, J.; Hanarp, P.; Sutherland, D. S.; Kall, M.; Bryant, G. W.; de Abajo, F. J. G. *Phys. Rev. Lett.* **2003**, *90*, 057401.
- (18) Nehl, C. L.; Liao, H.; Hafner, J. H. *Nano Lett.* **2006**, *6*, 683–688.
- (19) Sun, Y.; Xia, Y. *Science* **2002**, *298*, 2174–2179.
- (20) Halas, N. *MRS Bull.* **2005**, *30*, 363–367.
- (21) Prodan, E.; Nordlander, P.; Halas, N. J. *Nano Lett.* **2003**, *3*, 1411–1415.
- (22) Lassiter, J. B.; Aizpurua, J.; Hernandez, L. I.; Brandl, D. W.; Romero, I.; Lal, S.; Hafner, J. H.; Nordlander, P.; Halas, N. J. *Nano Lett.* **2008**, *8*, 1212–1218.
- (23) Neretina, S.; Hughes, R. A.; Britten, J. F.; Sochinskii, N. V.; Preston, J. S.; Mascher, P. *Nanotechnology* **2007**, *18*, 275301.
- (24) Neretina, S.; Hughes, R. A.; Devenyi, G. A.; Sochinskii, N. V.; Preston, J. S.; Mascher, P. *Nanotechnology* **2008**, *19*, 185601.
- (25) Draine, B. T. *Astrophys. J.* **1988**, *333*, 848–872.
- (26) Draine, B. T.; Flatau, P. J. *J. Opt. Soc. Am. A* **1994**, *11*, 1491–1499.
- (27) Draine, B. T.; Flatau, P. J. *DDSCAT 6.1*; Scripps Institute of Oceanography, University of California: San Diego, CA, 2005.
- (28) Draine, B. T.; Goodman, J. *Astrophys. J.* **1993**, *405*, 685–697.
- (29) Purcell, E. M.; Pennypacker, C. R. *Astrophys. J.* **1973**, *186*, 705–714.
- (30) Hu, M.; Chen, J. Y.; Li, Z. Y.; Au, L.; Hartland, G. V.; Li, X. D.; Marquez, M.; Xia, Y. N. *Chem. Soc. Rev.* **2006**, *35*, 1084–1094.
- (31) Kelly, K. L.; Coronado, E.; Zhao, L. L.; Schatz, G. C. *J. Phys. Chem. B* **2003**, *107*, 668–677.
- (32) Jain, P. K.; Lee, K. S.; El-Sayed, I. H.; El-Sayed, M. A. *J. Phys. Chem. B* **2006**, *110*, 7238–7248.
- (33) Lee, K. S.; El-Sayed, M. A. *J. Phys. Chem. B* **2005**, *109*, 20331–20338.
- (34) Noguez, C. *J. Phys. Chem. C* **2007**, *111*, 3806–3819.
- (35) Payne, E. K.; Shuford, K. L.; Park, S.; Schatz, G. C.; Mirkin, C. A. *J. Phys. Chem. B* **2006**, *110*, 2150–2154.
- (36) Yang, W. H.; Schatz, G. C.; Vanduyne, R. P. *J. Chem. Phys.* **1995**, *103*, 869–875.
- (37) Johnson, P. B.; Christy, R. W. *Phys. Rev. B* **1972**, *6*, 4370.
- (38) *Handbook of optical constants of solids*; Palik, E. D., Ed.; Academic Press: New York, 1998; Vol. 1.
- (39) Klimov, V. I.; Mikhailovsky, A. A.; McBranch, D. W.; Leatherdale, C. A.; Bawendi, M. G. *Science* **2000**, *287*, 1011–1013.

NL901960W